ARTICLE

Check for updates

Century-long column ozone records show that chemical and dynamical influences counteract each other

Stefan Brönnimann [1 ✉]

The recovery of the ozone layer, which is expected as stratospheric chlorine levels have decreased over the past 25 years, remains difficult to detect. Column ozone has been monitored from 1924 to 1975 in Oxford, UK. Here, I present a century-long Oxford column ozone record, extended to the present based on re-discovered material and neighbouring series, and analyse it together with a record from Arosa, Switzerland that starts in 1926. Neither series shows a clear increase over the past 25 years but suggest stratospheric circulation. I separate chemical and dynamical effects using a regression approach and find that chemical recovery amounts to +8 DU between peak stratospheric chlorine concentrations in 1997 to 2021, consistent with model simulations. However, this trend is counteracted by a −5 DU dynamical trend. Century-long ozone records provide a window to the past dynamical, chemical and radiative state of the stratosphere and help better constrain circulation effects on ozone recovery.

[1] Oeschger Centre for Climate Change Research and Institute of Geography, University of Bern, Bern, Switzerland. ✉email: Stefan.broenimann@giub.unibe.ch

The ozone layer is crucial for sustaining life on Earth's land surface. Its destruction by man-made chemicals was and still is a major environmental concern, as the expected recovery remains difficult to detect[1–3]. For a century, scientists have measured total column ozone (see Box 1)[4–6], which mainly represents stratospheric ozone. Today, the resulting long column ozone records could help us to assess ozone recovery and separate it from the effects of atmospheric circulation changes. Open questions concerning the contributions of ozone depleting substances, changes in ozone precursor gases, and climate change to changes in column ozone are mostly addressed with the help of models[7], but long records could help in the analysis. The record from Arosa, Switzerland, which starts in 1926, is the world's longest ozone record[8]. Another long record exists for Tromsø, Norway, reaching back to 1935[9]. In this contribution, I present a new, century-long ozone record for Oxford that reaches as far back as 1924. This series is based on existing segments[10], complemented with a new segment digitised from original data sheets from the 1970s (Fig. 1) and further extended to the present using series from neighbouring stations (see Methods).

The new series from Oxford is then analysed together with that from Arosa with respect to multiannual and long-term variability. Specifically, I use the long time series to better constrain ozone recovery and address trends in column ozone in the era prior to the onset of ozone depletion by chlorofluorocarbons.

Results

Comparison with other series. Figure 3 shows the new, centennial series from Oxford together with the series from Arosa as well as a 50-year long series of zonal mean total column ozone at 52.5°N from satellite instruments[11]. Note that the series are offset for visualisation (Arosa, 1000 km away from Oxford and at 1850 m asl has a lower ozone column than Oxford and both deviate from the zonal average). The two station series are in very good agreement. Both show the same long-term evolution, and they also show concurrent, strong spikes such as in the early 1940s or in 2010. The zonal average series also agrees well with the two station series. It shows less variability as zonally asymmetric effects of changes in the planetary wave structure and thus tropopause height partly cancel out. What remains are zonally symmetric, dynamical effects and chemical changes.

Box 1 | This history of column ozone monitoring

It is important to recall the history of column ozone monitoring in order to better understand the column ozone record. The existence of an ozone layer in the Earth atmosphere was proven by Fabry and Buisson[60] by measuring the spectrum of sunlight in the UV wavelength range. In 1920 they were able to quantify the amount of ozone as 3 mm and performed a short series of 14 measurements (see Fig. 2a)[58]. Their double spectrograph (with two dispersions at right angles to each other, used for the measurements plotted in Fig. 2a) successfully reduced stray light, but required a dedicated building and therefore was not convenient for monitoring or building up a network. In 1924, Dobson started measurements in Oxford with a simpler spectrophotographic instrument that could be used outdoors (Fig. 2b). He argued that the distribution of ozone in the atmosphere, given the various radiative properties, "may have important relations to other geophysical phenomena"[59]. During 1924, Dobson and Harrison tested the measurement set up—the earliest data point that made it to the publication[59] and to the global ozone data set dates to 18 August 1924—and then started regular observations.

Already Dobson's first measurements confirmed that total column ozone is a relevant meteorological quantity. Dobson and Harrison[59] found very strong correlations between total column ozone and pressure at the tropopause as measured with self-registering weather balloons (retrospectively, we find a relation between total column ozone and 200 hPa geopotential height (GPH) from a reanalysis[33] already in Fabry's data from 1920, see Fig. 2a). Consequently, Dobson quickly established a European network, which showed spatial changes in ozone that were related to weather systems[61]. After 2 years the instruments were redistributed; a global network gave a first view of the seasonal and latitudinal distribution of global ozone[62].

The close relation between total column ozone and upper-level flow was promising for meteorology, which at that time was discovering the relevance of the vertical dimension. Atmospheric profiles could possibly be beneficial for weather forecasts. However, no real-time data were available. The self-registering devices flown on weather balloons needed to be recovered after the burst of the balloon[63]. If column ozone could be measured in real time, then this could provide information on the tropopause-level flow. However, Dobson's apparatus registered the spectrum on photographic plates (Fig. 2b), which needed to be developed before measuring. Dobson, therefore, designed a photoelectric instrument which allowed quasi-real time observations[57]. However, at about the same time the radiosonde was invented, making Dobson's new instruments less interesting for weather forecasting. Several instruments were built, but then the Second World War put a halt to the plan of building up of a network equipped with the new instruments.

Although column ozone measurements could not support weather forecasting, the interest in stratospheric dynamics remained an important motivation to measure ozone, as chemical theories in the 1930s could not explain the latitudinal and seasonal distribution of stratospheric ozone[64,65]. Only a large-scale, meridional circulation that transports ozone away from its source region towards the winter hemisphere could explain the ozone distribution. This circulation, which was discovered in the 1940s and 1950s, is today known as the Brewer–Dobson circulation[66].

At the same time, new techniques (called "Umkehr") allowed retrieving profiles from ground-based observations[67]. Measurement techniques were further developed in Oxford and in France (e.g., through Arlette Vassy[68]). In the 1930s and 1940s, ozone became a geophysical quantity of scientific interest in its own right.

Within the International Geophysical Year in 1957/58, a global ozone monitoring network was established with improved Dobson instruments. The measurement principle has not changed since then, and instruments are still in use. The first space-borne sensors started to measure column ozone in the 1970s, starting a new era of column ozone observations[11].

With the discovery of the ozone hole in 1985[69], monitoring total ozone—now as an environmental indicator - became of utmost importance[70]. With the Brewer instrument[71], an automated total column instrument became available which now complements the global Dobson network (operated by Global Atmosphere Watch under the Global Ozone Observing System), together serving as a reference for satellite-based sensors. Ozone trends were a major research focus ever since[1,72]. Given the existing knowledge on the relation between total column ozone and upper-level flow, the dynamical contribution to ozone trends was studied extensively[39]. In the 1990s, the role of ozone as a radiative forcing agent of the climate system became an important additional aspect[73]. Today, in addition to observing the ozone layer (now with the task to monitor ozone recovery)[2], satellite measurements of total column ozone are assimilated into numerical weather prediction models, with the aim (among others) to improve weather forecasts[74]. Thus, the data are today used in a similar way as originally intended by Dobson in the 1920s.

The history of column ozone monitoring shows how the motivation behind measuring ozone changed several times. Observations continued, thus providing today a unique, long data set that can be used to address many different scientific questions.
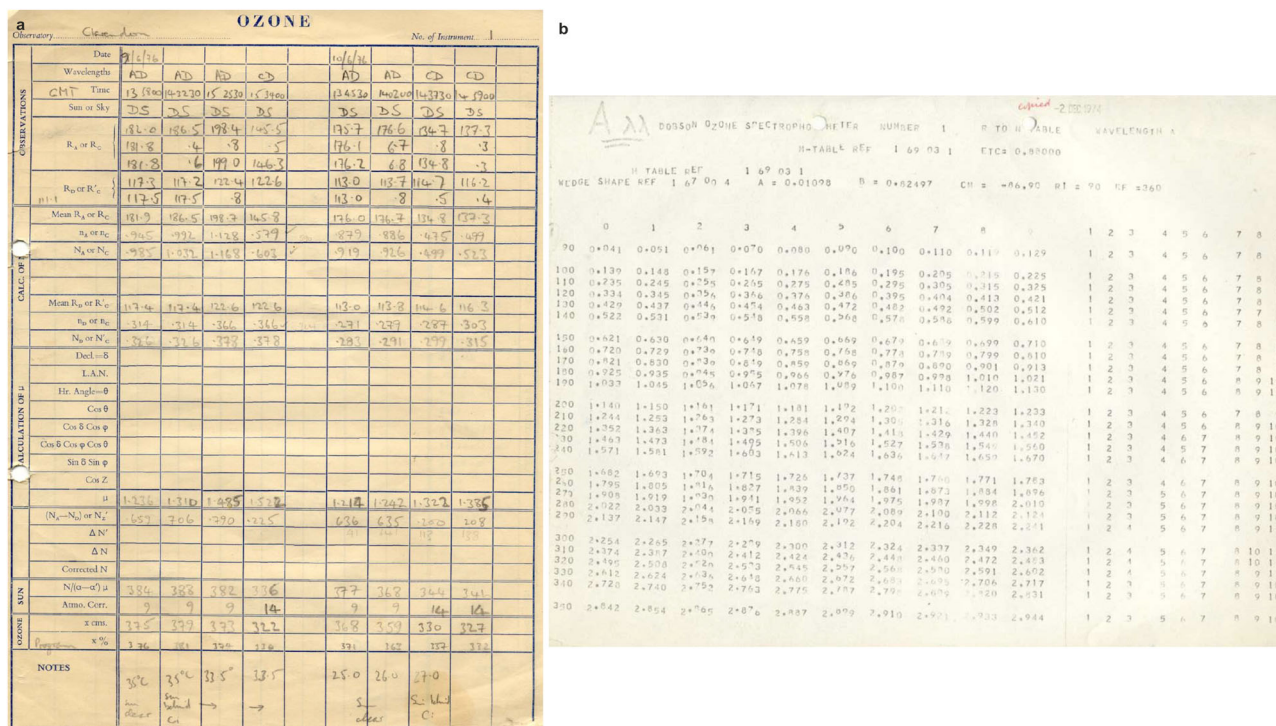

Fig. 1 Total column ozone observations sheets from Oxford. a Original observations sheet from Oxford, June 1976. **b** R-N table for the A pair, dated 1974 (excerpt).

Inter-and multiannual variability. The value of long records is that they capture a wider range of dynamical variability that affects the ozone layer. In the following, I focus on the two most prominent spikes in the two records, in the early 1940s and in 2010, and show that both can explained be exceptional, but different, atmospheric circulation. During the years 1940–42, total column ozone was exceptionally high over both stations. In fact, column ozone was also high at other locations in Europe, and also at stations on other continents (New York, Shanghai), as found in a previous study[12]. Here I add three further series, namely from Oxford, Table Mountain, California[13], and Montezuma, Chile (the latter two series are very sparse and based on spectroscopy in the visible wavelength range, i.e., the Chappuis band, which is much less accurate, see Methods). All extratropical series confirm the increase in 1940–1942 relative to the neighbouring years (Fig. 4), which is the expression of an increased transport of ozone from the tropics to the extratropics through a stronger Brewer–Dobson circulation. We would then expect an ozone decrease in the tropics. There is only one series from the tropics: Montezuma, Chile. Despite its very large uncertainty, it is interesting that this series shows a decrease concurrent with the increase in the extratropics.

The global view is analysed in a two-dimensional (latitude-height) ozone data set based on off-line assimilation of historical total column observations into a chemistry-climate model (HISTOZ[14]). Contrasting 1940–1942 with the neighbouring years, I find a decrease of ozone in the tropical lower stratosphere concurrently with the increase in the northern extratropics (Fig. 4, right), consistent with a large change in the Brewer–Dobson circulation (qualitatively depicted by long arrows in the figure), which was also found in model simulations[12,15]. Thus, historical total column ozone data, on an interannual time scale, can help to shed light on the variability of the stratospheric circulation.

The underlying cause of the strong Brewer–Dobson circulation, in this case, was an El Niño event, which was accompanied by a strong positive Pacific North American pattern and a negative phase of the North Atlantic Oscillation (NAO)[16]. These two variability modes might have contributed to enhanced wave-driving of the stratospheric circulation during this El Niño event[12,15] (short arrows in Fig. 4b). A weakened polar vortex[17] and increased poleward ozone transport during El Niño[18,19] was also found in other studies[20] (see also the review by ref. [21]). Conversely, the weak polar vortex caused by enhanced wave activity could have contributed, via downward propagation, to the cold European winters from 1940 to 1942.

This example shows that amplifications of the Brewer–Dobson circulation over 2–3 year are possible. This is relevant for assessing ozone trends, but also for better understanding stratospheric trace gas transport and the lifetime of stratospheric aerosols.

An even more prominent, but shorter change in total column ozone at the two stations occurred in 2010. This year's climate was also remarkable at the Earth surface in the North Atlantic-European sector. The NAO index reached the lowest recorded winter value, and Western Europe was in the grip of cold waves[16]. The stratospheric polar vortex (Fig. 5 shows 200 hPa height and anomalies with respect to 1991–2020, from ERA5[31]) started with many disturbances in November and December, but then was strong in early January[22]. A strong planetary wave number one event in the second half of January then led to a displacement of the vortex. From 22–26 January the situation developed into a sudden stratospheric warming due to a polar vortex split. The effects of this event (reversal of zonal mean wind in the stratosphere) lasted well into March, and polar-cap averaged temperatures of the stratosphere were high[22]. Monthly geopotential height anomalies at the tropopause over the polar cap remained positive (Fig. 5). The NAO index remained strongly negative during the entire year (with the exception of July, where the index reached +0.06[16]). Extremely low values were noted again in November and December of 2010. According to Steinbrecht et al.[23] the negative Arctic (or North Atlantic) Oscillation contributed ca. two thirds to the 2010 peak at
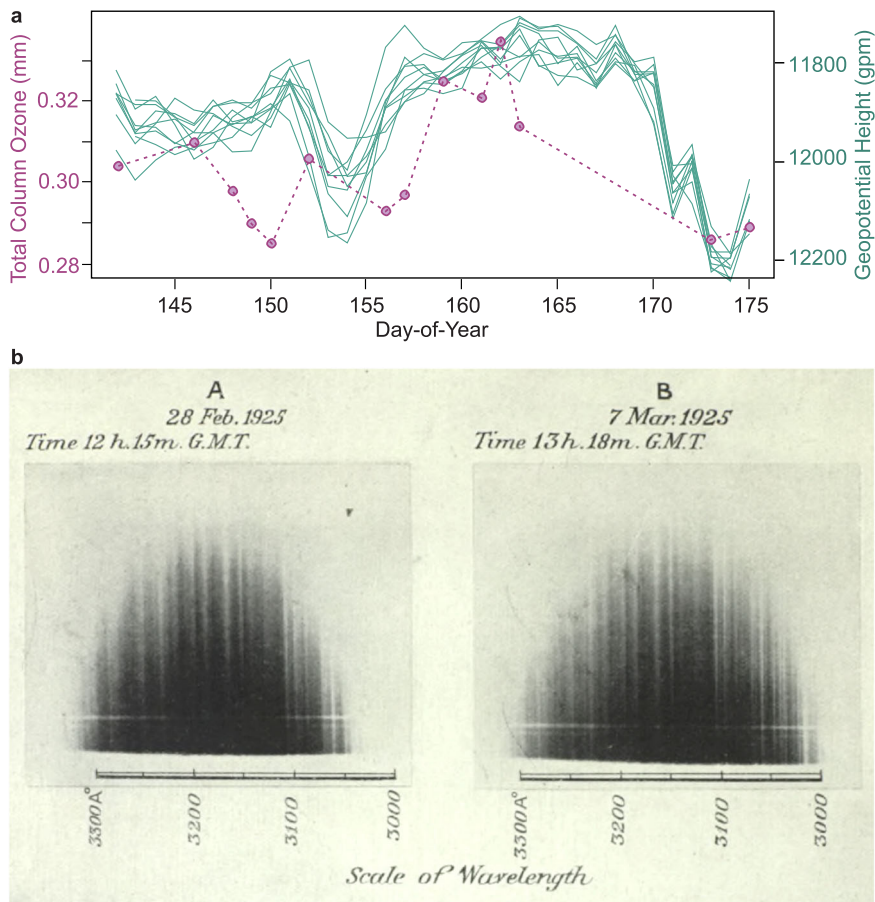
Fig. 2 The first total column ozone measurements. a Ozone measurements in Paris, May-June 1920 by Fabry and Buisson[58] (purple circles, given in their original units) and 200 hPa GPH from the CERA-20C reanalysis[33] (green lines, reverse scale, 10 ensemble members). **b** Photographed spectra in the UV region from which Dobson derived total column ozone by measuring the spectrum at wavelengths in which ozone absorbs relative to nearby wavelengths that are not absorbed (from Dobson and Harrison[59]).
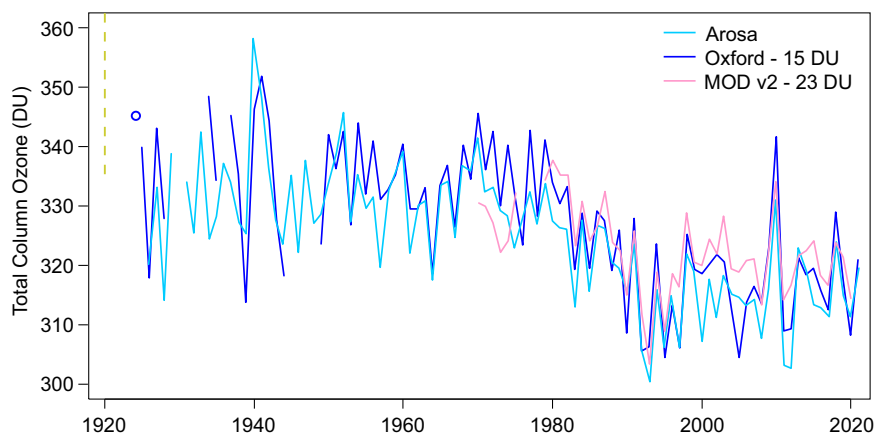

Fig. 3 Long-term total column ozone series. Annual mean total column ozone at Oxford (homogenised series), Arosa (continued with data from Davos after Feb 2021) as well as annual mean zonal mean total column ozone at 52.5°N from the SBUV merged data set MOD v2 from 1924 to 2021 (note the offsets). For historical reasons, I also plot the first data for Oxford, 1924 (blue circle) and Paris, 1920 (olive dashed line, qualitative), although requirements for annual averaging are not met.

Hohenpeissenberg, Germany. One third was attributed to an easterly wind-shear phase of the Quasi–Biennial Oscillation (QBO).

Oxford and particularly Arosa are near the southern centre of action of the NAO and therefore ozone anomalies are expected in relation to NAO excursions[24]. Monthly anomalies at Oxford (i.e.,

Reading) and Arosa relative to 1991–2020 were positive in each month of 2010, strongest in December (Fig. 5). This is a different situation than in the early 1940s as it is rather connected to an unusual persistence of the geopotential height anomaly pattern.

Very strong variations such as 1940–1942 and 2010 need to be understood for assessing ozone trends[24] and for detecting ozone
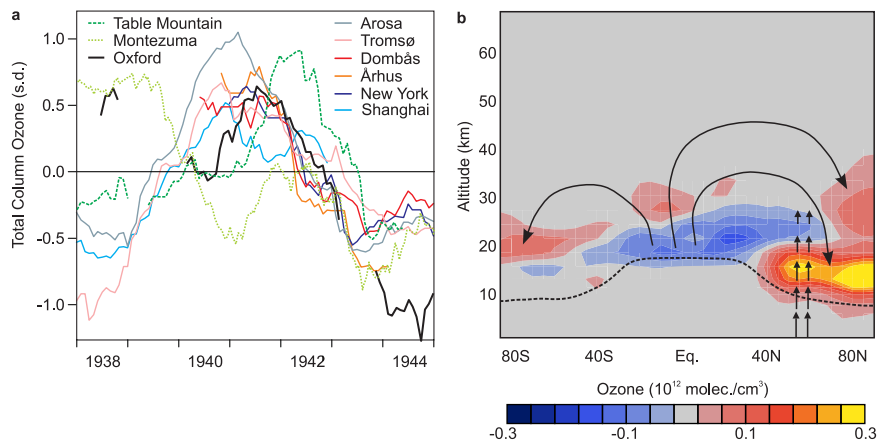
Fig. 4 Stratospheric ozone during the early 1940s. a Total column ozone (standardised anomalies with respect to 1938–1944) at nine stations smoothed with a 12-month moving average (see Methods)[12]. **b** Zonally averaged ozone concentrations from HISTOZ[14] in 1940–1942 (annual means of ensemble mean) relative to the annual averages of 1938, 1939, 1943, and 1944. The long arrows qualitatively indicate the strengthening of the Brewer–Dobson circulation, the short arrows the wave-driving of stratospheric circulation, the dotted black line indicates the tropopause.

Table 1 Changes in column ozone in different periods (in DU over the entire period) in observations and in different terms of the regression model (linear least-squares fit with 95% confidence intervals; for uncertainty of regression coefficients see Fig. 7).

Station	Period	Observations	Fit	Chemistry	Dynamics	Residuals
Oxford	1997–2021	0.71 ± 10.46	3.99 ± 6.73	8.09 ± 1.13*	−4.09 ± 6.52	−3.29 ± 7.86
Arosa	1997–2021	2.47 ± 8.87	3.01 ± 6.70	8.03 ± 0.69*	−5.02 ± 6.73	−0.54 ± 6.27
Oxford	2000–2021	0.06 ± 11.10	1.16 ± 6.83	6.84 ± 1.22*	−5.68 ± 6.71	−1.10 ± 8.73
Arosa	2000–2021	3.67 ± 9.31	0.59 ± 7.08	6.93 ± 0.76*	−6.34 ± 7.17	3.09 ± 6.38
Oxford	1926–1960	2.28[a]	3.93 ± 5.95	3.89 ± 1.16*	0.05 ± 5.89	−2.52 ± 12.09
Arosa	1926–1960	3.89 ± 10.12	4.04 ± 5.77	3.02 ± 0.74*	1.02 ± 5.79	0.76 ± 7.38
Oxford	1926–1970	0.19[a]	2.62 ± 5.61	1.50 ± 1.56	1.12 ± 5.39	−2.80 ± 9.05
Arosa	1926–1970	1.53 ± 8.62	2.17 ± 5.42	0.90 ± 1.25	1.27 ± 5.24	0.16 ± 5.80

Significant coefficients are marked with *($p < 0.05$)
[a]No confidence interval is given as during this period, inhomogeneities in the Oxford record were corrected.

recovery. In the next section, a regression model is used to capture these effects and separate them from chemical effects.

Long-term trends. Both series, Arosa and Oxford, exhibit their lowest values in 1992 or 1993, after the Pinatubo eruption and at a time with high stratospheric chlorine loading (Fig. 3). Ozone recovery was then expected. However, almost 30 years later, ozone columns have not increased strongly. Since 1997, when stratospheric chlorine concentration peaked[25], column ozone increased only 1–2 DU until 2021, similar numbers are found for the period since 2000 (Table 1; note the Oxford column ozone data 2002–2021 are from Reading, those before 2002 are from Camborne and adjusted to Reading; the effect of this change on the trend since 2000 is likely small).

In order to detect recovery, long records are vital[26] not only because they reach back into the "pre-CFC" period, but also because they cover, compared to short series, a larger range of circulation-related anomalies such as those in the early 1940s and 2010. Long-term trends such as those arising from ozone depleting substances or those due to climate change or changing emissions of ozone precursor gases can then be better isolated. I formulated multiple linear regression models to explain the time series of annual mean column ozone, with predictor variables that capture chemical as well as dynamical effects (though a strict separation is not possible). Five chemical variables were considered. Ozone depletion is measured by the Equivalent Effective Stratospheric Chlorine (the variable is termed EESC)[27].

The time series for the midlatitudes, starting in 1960, is backward extended asymptotically to plateau out in 1950 and updated after 2008 based on ref. [25]. The concentration of methane[28] is used as a proxy for chemical ozone formation from precursor gases. The CO_2 concentration[28] is taken as a measure of upper-stratospheric cooling, causing higher ozone concentrations. The global aerosol optical depth[28,29] (VOL) is used to measure ozone depletion due to volcanic aerosols. Finally, spectral solar irradiance in the 240–280 nm band represents the chemical effect of solar UV changes[30]. All data were used in the form of annual mean values.

In addition to chemical variables, I considered three dynamical variables. The QBO was incorporated as the May-to-October average zonal mean zonal wind at 50 hPa, which was found to give the best fit. QBO data were taken from ERA5[31] after 1979 and from a reconstruction[32], adjusted to ERA5 based on the 1979–2010 overlap, for 1925–1978 (this reconstruction is itself based on ERA40 between 1957 and 1978). I also included the strength of the polar vortex at 200 hPa (POL, defined as the difference between geopotential height at 75–90°N and 45–55°N[32]) from ERA5 back to 1950, backward extended with CERA-20C data[33] (adjusted to ERA5 based on the 1950–1956 overlap), averaged from December (of the preceding year) to April. This is the season when the large-scale stratospheric circulation is most active and ozone most variable and when the polar vortex is most closely related to the Brewer–Dobson circulation[34]. In this way, the state of the polar vortex can imprint on the entire year as anomalies at the end of the winter tend to persist for several months[35]. I also considered local 200 hPa
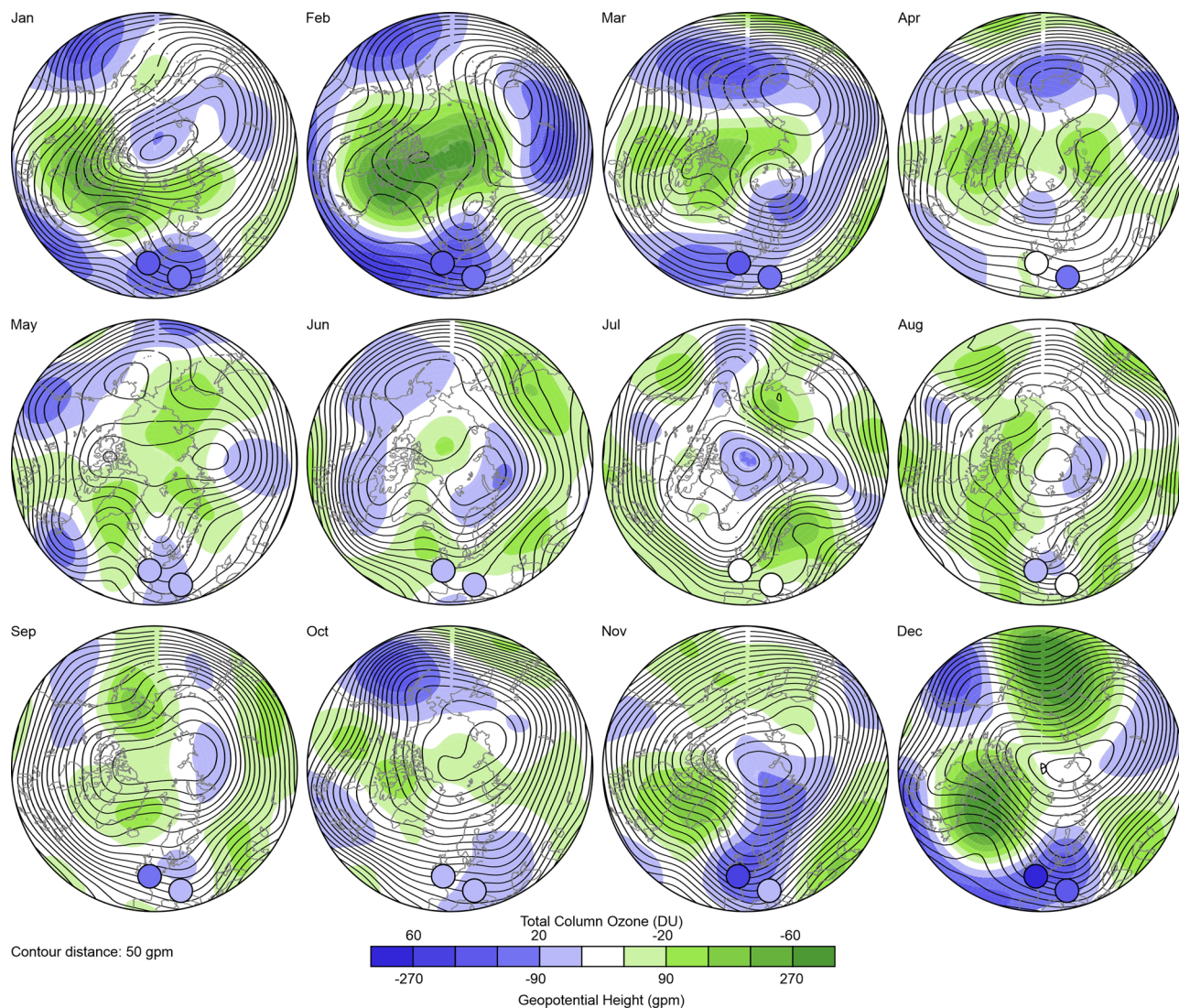
5

Fig. 5 Upper-level circulation and ozone in 2010. 200 hPa geopotential height (lines) and anomalies (shading) from the 1991–2020 mean in each month of 2010 (ERA5 data). Also shown are total column ozone anomalies at Arosa and Oxford (filled circles).

height (Z200) as a measure of local tropopause height. A low tropopause is associated with a larger fraction of stratospheric air in the column and therefore higher column ozone, exactly as found by Dobson in 1924 (shown in Fig. 2) and in the extreme year 2010 (Fig. 5). This is a year-round, instantaneous effect and hence the annual mean is chosen. Data are taken from ERA5 back to 1950, backward extended with a reconstruction based on upper air observations[36] (individual missing months were complemented with CERA-20C, all data were adjusted to ERA5 based on the 1950–1956 overlap). This replaces the use of an NAO index as in other approaches[37]; in fact, including an annual mean NAO[16] in addition to Z200 does not improve the result, using it instead of Z200 makes results clearly worse. Finally, in line with other regression approaches[37], I also tested a predictor for the effect of El Niño (ENSO), namely the NINO3.4 index from HadSST1, averaged from September of the previous year to February[38]. However, as for the NAO, the effect is sufficiently well captured by the other dynamical variables. Unfortunately, eddy heat fluxes or similar measures of the strength of the Brewer–Dobson circulation are not available back to 1924. Note that only Z200 is different between Arosa and Oxford. Due to tropospheric warming, Z200 has a trend that might affect column ozone

partly dynamically[39] but might not separate well from chemical variables in the regression.

Regression results (least-squares fit) show that most of the variables have coefficients that are significantly different from zero at Arosa or Oxford. Exceptions are CO_2, which also has an unexpected negative sign at both locations (arguably due to collinearity with CH_4) and is highly collinear with the other variables, and solar UV. Therefore, I excluded CO_2 but kept solar UV (termed SOL) as it has the correct (positive) sign and collinearity is not a problem. Note that methane (termed GHG) and EESC, though both significant, still have a high degree of collinearity.

The final models have seven predictor variables. The explained variance amounts to 69% for Oxford and 79% for Arosa; coefficients are given in Supplementary Table S1. The correlation between the two column ozone time series decreases from 0.87 in the observations to 0.62 in the residuals. This implies that there is common unexplained variability that could possibly be explained with better or additional predictor variables or more complex, monthly models, which however would come at the cost of simplicity (also, observations at Oxford were taken irregularly, such that monthly means could often not be calculated). Errors
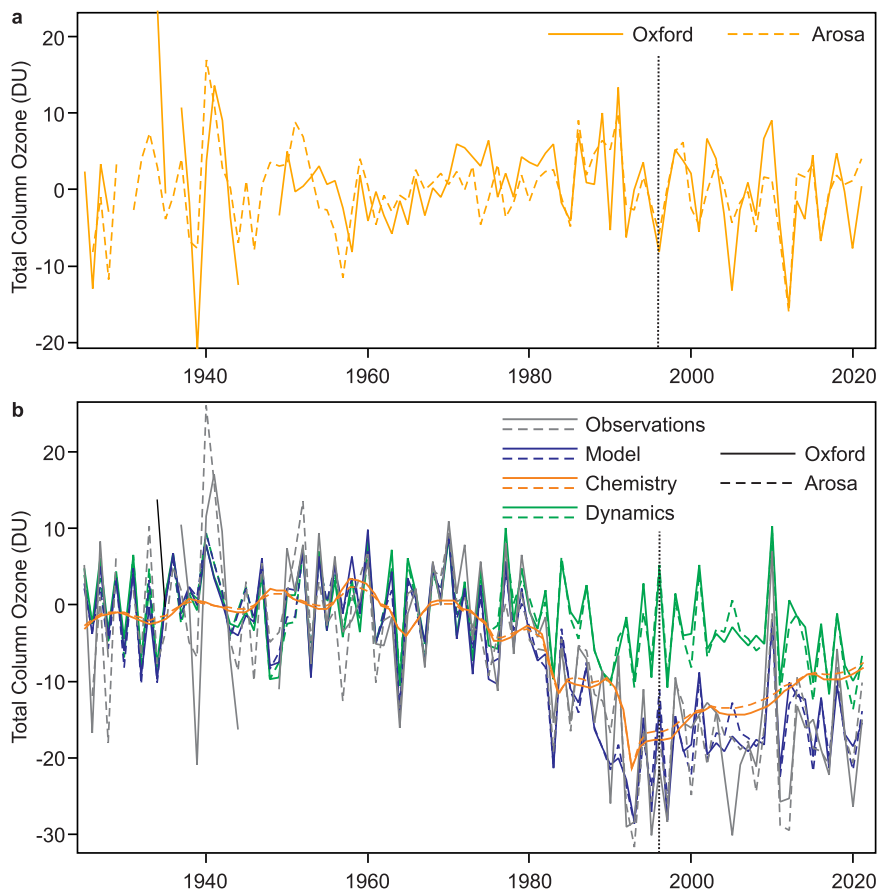
Fig. 6 Components of the regression fit for Oxford and Arosa. a Residuals and **b** sum of chemical and dynamical variables as well as observations and model fit. For visualisation, series are centred around their 1924–1960 mean value. The dotted black line marks the year 1997.

and uncertainties in the ozone data and in the predictor data contribute to unexplained variance.

The residuals of both models (Fig. 6a) show no specific patterns, apart from a high value at Oxford in 1934 (which is based on very few observations, but fulfils the criteria defined). The two prominent excursions in the 1940s and in particular in 2010 are greatly reduced in the residuals, indicating that the model well captures dynamical effects (for the 2010 case, Z200 and QBO explain roughly equal proportions of the anomaly at Oxford and Arosa relative to the neighbouring years, comparable to the results of ref. [40]). No long-term trend is visible in the series and there is no autocorrelation. I can therefore interpret the model.

The chemical and dynamical contributions, each centred around the period 1924–1960 (pre-CFC era) for visualisation, are shown in Fig. 7. Oxford (solid) and Arosa (dashed) agree well. The contribution with the largest amplitude in both models is EESC, followed by methane. Volcanic eruptions also had a marked impact. The dynamical contributions (Fig. 7b) have smaller amplitudes than the chemical ones, obviously varying strongly from year to year. The magnitude of all three dynamical contributions is similar, and they are almost identical for Oxford and Arosa.

The fitted values (Fig. 6b) track the observations well. They also show a small but non-significant increase since 1997 (Table 1, for comparison with the LOTUS[37] (Long-term Ozone Trends and Uncertainties in the Stratosphere) activity the Table also provides trends since 2000, which yields very similar results). This is however not true for the chemical and dynamical contributions individually. The sum of the chemical contributions reaches a

minimum after the Pinatubo eruption and shows a clear increase afterwards. Since 1997, column ozone would have increased by 8 DU (1% decade^{-1}) (Table 1, 7 DU since 2000) until 2021 due to a decrease in stratospheric chlorine and an increase in methane or other ozone precursors and upper-stratospheric recovery. Conversely, the sum of the dynamical contributions shows a decrease of ca. 4–5 DU or 0.5% decade^{-1} (Table 1, 6 DU since 2000). This negative dynamical trend, whose coefficient is not statistically significant at the 95% significance level, hides the increase expected from the chemical contribution.

Finally, I also performed the same analysis for the periods 1926–1960 and 1926–1970, i.e., periods during which the effect of stratospheric chlorine was weak. For the former period I find an increase of ca. +3 DU (0.25% decade^{-1}) in the observations, which is reproduce in the regression model (ca. 4 DU) and is due to chemistry (3.5 DU). The latter period shows no trend in observations, +2.5 DU in the model with contributions of chemistry and dynamics of 1 DU. These trends are all very small and not significant.

Discussion
Column ozone monitoring has a century-long history (see Box 1). However, up to now only two long records have been available[8,9]. All other long series start in 1957 or later (see ref. [41] for an overview of ground-based measurements and their role in studying ozone recovery). The new Oxford series is therefore a welcome addition and provides support for the Arosa record, which is arguably of higher quality. Together, the two series allow us to analyse past variability and to better assess trends.
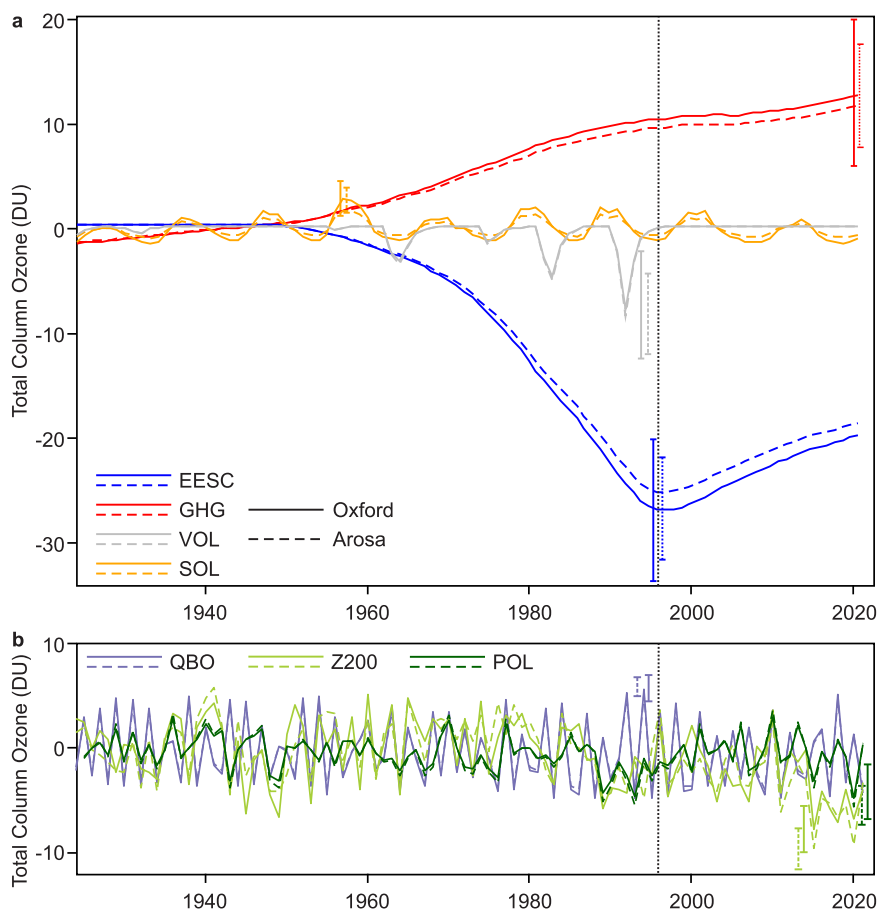
Fig. 7 Components of the regression fit for Oxford and Arosa. a Chemical variables and **b** dynamical variables. For visualisation, series are centred around their 1924–1960 mean value. Error bars indicate ±1 standard error of the coefficients, multiplied with (and shown at the location of) the maximum absolute anomaly from the mean over the time series of the corresponding predictor variable. The dotted black line marks the year 1997.

Neither series shows a significant trend since the peak of stratospheric chlorine. This is in agreement with several other studies[37,42–44]. Coldewey-Egbers et al.[44] find regionally different trends (1995–2020) that are positive ($1.5 \pm 1.0\%$ decade^{-1}) over the North Atlantic and negative ($-1.0 \pm 1.0\%$ decade^{-1}) over Eastern Europe and are modulated by long-term changes in tropopause pressure. My study suggests that, for an unchanged circulation, ozone over Oxford and Arosa would possibly have increased by 8 DU since 1997, which is in agreement with changes found in chemistry-climate models[40,45]. This trend is masked by a negative trend of -5 DU induced by atmospheric circulation. This is consistent with Weber et al.[43], who found a positive trend after 1996 only when properly accounting for dynamical changes. All three of our predictors (local tropopause height, polar vortex strength, and the Quasi–Biennial Oscillation) contribute to this negative trend; the first contributed the most. Together they offset almost two thirds of the chemically induced increase over the past 25 years. The warming troposphere and the poleward shift of atmospheric circulation might contribute to the trend in Z200 and continue into the future. However, the trend in the dynamical contribution is not statistically significant in my model and thus could also partly reverse in the future. The recovery of the ozone layer is a slow process, the amplitude over the past quarter century is likely small and thus circulation variability – random or not – can hide the trend at a given location[3]. Long time series can help to better address and put into perspective the dynamical contributions.

However, the statistical model used in this study has uncertainties. Calibrating statistical models mainly in the phase of

ozone depletion can lead to misleading results[46]. By taking a century-long perspective, the regression in this study should be more robust, but stationarity is still assumed. The fact that we now have two long records, whose coefficients are very similar, and that all coefficients have the theoretically expected sign also suggests that the results are robust. The regression model could possibly be further improved[37] by including seasonally varying factors or allowing for non-linear relations. Furthermore, the predictor variables themselves have uncertainties, particularly in the early decades.

Some factors need additional study. The trend in column ozone is affected by changes in tropospheric ozone. At temperate latitudes surface ozone increased by 30–70% between the historical period (1896–1975) and the present (1990–2014)[47], the increase in the tropospheric column is however difficult to estimate. In the regression model, this trend would be captured by the increasing methane concentrations. However, these contribute only to a small chemical column ozone increase from the 1920s to the 1960s, amounting to ca. 2–4 DU. Interestingly, an increase in total column was noted by ozone scientist at that time[48]. In CMIP6 models column ozone at 30°–60°N increases by ca. 4–5% (ca. 12 DU) from the 1920s to 1960s[40], which is considerably more than in my regression model (0–1% or 0–4 DU, Table S1) and cannot be explained with uncertainties in the regression coefficients. An increase of ca. 3% from pre-industrial to present day due to increasing precursor gases is found in another study[7]. These different numbers point to the need of reconciling climate model simulations with historical observations. Specific model studies would be needed to clarify these important discrepancies.

With respect to chemical processes in the stratosphere, recent studies show that there can still be surprises[49]. Long time series are required for better addressing these questions. Although long series are only available for the northern midlatitudes and do not allow conclusions on global recovery, they allow testing the results from chemistry-climate model simulations. This study shows a good agreement for the recovery period (1997–2021), but a worse agreement for the pre-CFC era (1926–1970).

Historical ozone data also serve as a diagnostic for past atmospheric circulation changes, as shown on behalf of the 1940–1942 anomaly. They have been used for that purpose since the early years (see Box 1). The Brewer–Dobson circulation was discovered in the context of studies on the global ozone distribution. Total column ozone played a role in our understanding of the Quasi–Biennial Oscillation from the very start[50]. More recently, total column ozone data were used in one of the first studies on the expansion of the tropical belt[51], and historical total column ozone data were used to study the preceding southward shift of the northern tropical belt[52].

Therefore, historical ozone data can help us to better understand past weather and climate extremes. Long series cover a broader range of circulation-related anomalies and serve as a background against which ozone trends can be compared. In this study, the analysis of past events suggests that deviations of 20–30 DU over 2–3 years are possible. Even the day-to-day changes could be informative. Historical column ozone measurements could today lead to improved weather reconstructions by assimilating them into reanalyses, thus using them in a similar way as envisaged by Dobson in 1924.

Ozone monitoring has a century-long history that goes back to the work of Fabry in Paris and Dobson in Oxford. The interest in ozone has changed several times – ozone was a meteorological quantity, then a geophysical quantity, a chemical quantity, and a radiative quantity – evidencing the many geophysical relations it has with the atmosphere (the motivation of Dobson back in 1924, see Box 1). For precisely these reasons, historical ozone data are interesting today as a window to the past radiative, dynamical and chemical state of the atmosphere, with relevance for answering currently open questions in science such as constraining ozone recovery.

Methods

Oxford ozone series. The Oxford record from 1924 to December 1975 has been re-evaluated by ref. [10]. These data were obtained by or under the direct guidance of G. M. B. Dobson and they are available from the World Ozone and Ultraviolet Radiation Data Centre (WOUDC, https://woudc.org). Dobson died on 11 March 1976. Here, I add two more years of data that were measured by the staff of the Department, including Robert J. Wells, after Dobson's death, covering June 1976 to October 1977. The instrument used was still the same – Dobson Spectrophotometer #1. These data were digitised from the original data sheets (Fig. 1) and processed according to the Handbook for Dobson Ozone Data Re-evaluation (see next Section)[53]. In total, 1209 measurements were digitised. There are some gaps in the extremely hot summer of 1976 as the instrument got too hot.

Most observations used the AD or CD wavelength pairs, some were done with the CC' pair. Operation modes include the standard modes direct sun (DS), zenith blue (ZB), and zenith cloudy (ZC). In addition, modes MS, FS, and FSF are marked on the data sheets. FS and FSF possibly refer to "focused sun" and "focused sun with filter" observations. The latter were exclusively performed when the sun was very low.

Processing. In Dobson spectrophotometers, ozone x is calculated from the radiation intensities I at two wavelengths λ and λ' via the relative intensity N:

$$N = \log\left(\frac{I_0}{I_0'}\right) - \log\left(\frac{I}{I'}\right) \tag{1}$$

where I and I_0 are the intensities at the surface and outside the Earth's atmosphere, respectively. N is normally obtained from the dial reading at the instrument, R, via an instrument specific conversion table (R-N table). Observations mostly use the double difference of two wavelength pairs (subscripts 1 and 2), the standard

equation for calculating total column T ozone then is:

$$T_{12} = \frac{(N_1 - N_2) - [(\beta - \beta')_1 - (\beta - \beta')_2]\frac{mp}{p_0} - [(\delta - \delta')_1 - (\delta - \delta')_2]\sec(SZA)}{[(\alpha - \alpha')_1 - (\alpha - \alpha')_2]\mu} \tag{2}$$

where β is the Mie scattering coefficient (primes denote the longer wavelength), α is the absorption coefficient, δ is the aerosols scattering coefficient, m is the relative air mass, μ is the relative path length through the ozone layer, SZA is the solar zenith angle, p is station pressure, and p_0 is mean sea-level pressure.

Aerosol scattering can then be neglected and the equation reduces to:

$$T_{12} = \frac{(N_1 - N_2) - [(\beta - \beta')_1 - (\beta - \beta')_2]\frac{mp}{p_0}}{[(\alpha - \alpha')_1 - (\alpha - \alpha')_2]\mu} \tag{3}$$

From the observation time I recalculated the solar zenith angle and, assuming a mean ozone layer height of 22 km, the air mass m and the relative path length through the ozone layer μ. I used pressure data from E-Obs[54] for p in Eq. 3. In addition to the data sheets, I also have the R-N table for this instrument, dated to 1974 (Fig. 1). The data sheets indicate intermediate steps, allowing in part to reverse engineer the calculations, but the intermediate steps become more sparse as time progresses, and soon only the dial readings R and the final ozone values are noted. From the observations with intermediate steps, I note that the R-N table was not applied directly, but offsets of 0.040, 0.024, and 0.012 were added for the A, C, and D wavelength pairs. However, the ozone values derived in this way (those reduced by the observers as well as my re-calculation) showed quite substantial differences between concurrent (<1 h apart) DS measurements at the AD and CD pairs, amounting to ca. 15 DU. I considered the AD pair as the standard and changed the offset applied to the C pair to 0.034, such that the differences vanished ($r = 0.97$, RMSE = 12 DU). I then reduced all other operation modes based on their N and μ values according to simultaneous measurements with already reduced data as described below.

First, I reduced the MS measurements. In the original calculations offsets of -0.121, -0.076, and -0.025 were applied for the A, C, and D pairs. However, results showed a rather poor agreement with DS measurements (both AD or CD). Therefore, I used a regression model as suggested by ref. [55]

$$x = c_0 + c_1 N + c_2 \mu + c_3 N^2 + c_4 \mu^2 + c_5 N^3 + c_6 \mu^3 + c_7 N\mu + c_8 N\mu^2 + c_9 N^2\mu \tag{4}$$

This regression was calibrated separately for AD-MS vs. AD-DS ($R^2 = 0.988$, RMSE = 5 DU) and CD-MS vs. CD-DS ($R^2 = 0.977$, RMSE = 7 DU) data. The FS observations were reduced using the R-N conversions of the DS values. I found a bias of -7.8 DU (RMSE = 10 DU) for AD-FS and -7.8 (11) DU for CD-FS, which I considered acceptable. Then AD-ZB data were reduced to AD-DS (using Eq. 4) after removing 2 outliers ($R^2 = 0.991$, RMSE = 3.6 DU). AD-FSF and CD-FSF were separately reduced, however, due to the smaller number of simultaneous observations, both were reduced against all AD/CD DS/MS measurements combined ($R^2 = 0.985$, RMSE = 6.3 DU, for AD-FSF and $R^2 = 0.987$, RMSE = 6.1 DU, for CD-FSF).

Then I reduced CC' ZB (against AD-DS), yielding $R^2 = 0.908$, RMSE = 13 DU. CC' ZC data could not be reduced in the standard way as no N-values were given for the C' pair, only R values. Therefore, I used polynomial regression (against all AD/CD DS/MS data as there were too few simultaneous AD-DS observations):

$$x = c_0 + c_1 N + c_2 \mu + c_3 R_{C'} + c_4 N\mu + c_5 N R_{C'} + c_6 \mu R_{C'} + c_7 N^2 + c_8 \mu^2 + c_9 R_{C'}^2 \tag{5}$$

This model yields $R^2 = 0.946$, RMSE = 14 DU. Finally, values from different observation modes and wavelengths were then averaged to yield daily ozone data. Given the RMSE values from the comparison above (to which both compared series contribute) and given the fact that daily means typically average ca. 3 values, thus reducing the random error, we can assume that the error of daily values is clearly below 10 DU.

Homogenisation. After 1977, I complemented the Oxford series with data from Bracknell (1967–1989, Dobson Beck #2, 65 km from Oxford), Camborne (1989–2003, Dobson Beck #41, 330 km), and Reading (2002–2021, Brewer MkIV #75, 38 km), all taken from the WOUDC. All series were statistically adjusted to the Reading series by adding offsets based on the overlapping data portions and proceeding backwards (no adjustment was performed for the transition from Bracknell to Camborne, which do not overlap). For annual averaging, to make best use of sparse data, I deseasonalised the data by fitting and subtracting the first two harmonics of the annual cycle and adding back the constant (mean value). This was performed separately for each daily value considering a window of ±500 values (correspondingly shortened at the edges). Then I averaged the data into 5-day intervals. If at least 15 intervals were available in a given year, an annual average was formed. The same procedure was applied to the homogenised series from Arosa. Applying the Craddock test[56] revealed a clear break in 1963, the cause could not be identified. The break was corrected by considering 5 years before and after the break. Furthermore, the period 1933–1946 (in this period Dobson used his photoelectric instrument[57], but not yet with a photomultiplier) was found to be off

and was adjusted to the period 1949–1962 (note that this period is internally rather heterogeneous; further subdivisions would be equally defendable).

Total column ozone in 1938–1944. Three series were added to the figure of Brönnimann et al.[12]: Oxford, Table Mountain[13], and Montezuma. From the monthly means in 1938–1944 in the Oxford series, the mean annual cycle was subtracted, the anomalies were standardised and smoothed with a 12-month moving window. For Oxford, a minimum of 10 daily values per month and 6 monthly means per 12-month average was required. I also added ozone data calculated from transmission in the visible wavelength range at Table Mountain, California (at 574 and 615 nm) and Montezuma, Chile (at 578 nm). As these measurements were very sparse, I processed daily data and subtracted an annual mean cycle based on fitting the first two harmonics of the annual cycle and then standardising the daily anomalies. To produce a 12-month moving average, I required 15 daily values per window (due to the different method the lines are dashed).

Data availability
The ozone data are available in the Supplementary Data and is also available from https://doi.org/10.6084/m9.figshare.19698274. Additionally, the new Oxford data have been sent to WOUDC (https://woudc.org/), where they will be available. Ozone data for Arosa, Bracknell, Cambourne, Oxford and Reading are available from WOUDC (https://woudc.org). The predictor variables used in the regression model are given in the Supplementary Data and are also available from https://doi.org/10.6084/m9.figshare.19698274. ERA5 data are available from the Copernicus Climate Data Store (https://cds.climate.copernicus.eu/#!/home). QBO data can be downloaded from the KNMI Climate Explorer (https://climexp.knmi.nl/start.cgi) Upper-air-based reconstructions of geopotential height can be downloaded from https://www.palaeo-ra.unibe.ch/data_access/. The HISTOZ assimilated ozone data set is available from https://boris.unibe.ch/71600/. The source data underlying the figures in this paper are available from https://doi.org/10.6084/m9.figshare.19721539.v1. The MOD v2 BUV data can be downloaded from NASA (https://acd-ext.gsfc.nasa.gov/Data_services/merged/index.html).

Code availability
The code to process the ozone data is available in the Supplementary Data and is also available from https://doi.org/10.6084/m9.figshare.19698274.

References
1. Solomon, S. Stratospheric ozone depletion: A review of concepts and history. *Rev. Geophys.* **37**, 275–316 (1999).
2. Solomon, S. et al. Emergence of healing in the Antarctic ozone layer. *Science* **353**, 269–274 (2016).
3. Steinbrecht, W., Hegglin, M. I., Harris, N. & Weber, M. Is global ozone recovering? *Comptes Rendus Geoscience* **350**, 368–375 (2018).
4. Stolarski, R. S. History of the study of atmospheric ozone. *Ozone Sci. Eng.* **2**, 421–428 (2001).
5. Müller, R. A brief history of stratospheric ozone research. *Meteorol. Z.* **18**, 3–24 (2009).
6. Bojkov, R. D. *International Ozone Commission: History and activities*. IAMAS Publication Series No. 2 (2012).
7. Reader, M. C., Plummer, D. A., Scinocca, J. F. & Shepherd, T. G. Contributions to twentieth century total column ozone change from halocarbons, tropospheric ozone precursors, and climate change. *Geophys. Res. Lett.* **40**, 6276–6281 (2013).
8. Staehelin, J. et al. Total ozone series at Arosa (Switzerland): Homogenisation and data comparison. *J. Geophys. Res.* **103**, 5827–5841 (1998).
9. Hansen, G. & Svenøe, T. Multilinear regression analysis of the 65-year Tromsø total ozone series. *J. Geophys. Res.* **110**, D10103 (2005).
10. Vogler, C., Brönnimann, S., Staehelin, J. & Griffin, R. E. M. The Dobson total ozone series of Oxford: Re-evaluation and applications. *J. Geophys. Res.* **112**, D20116 (2007).
11. Ziemke, J. R. et al. A global ozone profile climatology for satellite retrieval algorithms based on Aura MLS measurements and the MERRA-2 GMI simulation. *Atmos. Meas. Tech.* **14**, 6407–6418 (2021).
12. Brönnimann, S. et al. Extreme climate of the global troposphere and stratosphere in 1940-42 related to El Niño. *Nature* **431**, 971–974 (2004).
13. Brönnimann, S. Interactive comment on "Detection and measurement of total ozone from stellar spectra: Paper 2. Historic data from 1935–1942" by R. E. M. Griffin. *Atmos. Chem. Phys. Disc.* **5**, S4045–S4048 (2005).
14. Brönnimann, S. et al. A global historical ozone data set and signatures of El Niño and the 11-yr solar cycle. *Atmos. Chem. Phys.* **13**, 9623–9639 (2013).
15. Fischer, A. M. et al. Stratospheric winter climate response to ENSO in three chemistry-climate models. *Geophys. Res. Lett.* **35**, L13819 (2008).
16. Osborn, T. J. Winter 2009/2010 temperatures and a record-breaking North Atlantic Oscillation index. *Weather* **66**, 19–21 (2011).
17. Garfinkel, C. I. & Hartmann, D. L. Different ENSO teleconnections and their effects on the stratospheric polar vortex. *J. Geophys. Res.* **113**, D18114 (2008).
18. Cagnazzo, C. et al. Northern winter stratospheric temperature and ozone responses to ENSO inferred from an ensemble of Chemistry Climate Models. *Atmos. Chem. Phys.* **9**, 8935–8948 (2009).
19. Rieder, H. E. et al. On the relationship between total ozone and atmospheric dynamics and chemistry at mid-latitudes. Part 2: The effects of the El Niño/Southern Oscillation, volcanic eruptions and contributions of atmospheric dynamics and chemistry to long-term total ozone changes. *Atmos. Chem. Phys.* **13**, 165–179 (2013).
20. Brönnimann, S. et al. The 1986–1989 ENSO cycle in a chemical climate model. *Atmos. Chem. Phys.* **6**, 4669–4685 (2006).
21. Domeisen, D. I., Garfinkel, C. I. & Butler, A. H. The teleconnection of El Niño Southern Oscillation to the stratosphere. *Rev. Geophys.* **57**, 5–47 (2019).
22. Dörnbrack, A. et al. The 2009–2010 Arctic stratospheric winter—general evolution, mountain waves and predictability of an operational weather forecast model. *Atmos. Chem. Phys.* **12**, 3659–3675 (2012).
23. Steinbrecht, W. et al. Very high ozone columns at northern mid-latitudes in 2010. *Geophys. Res. Lett.* **38**, L06803 (2011).
24. Appenzeller, C., Weiss, A. K. & Staehelin, J. North Atlantic oscillation modulates total ozone winter trends. *Geophys. Res. Lett.* **27**, 1131–1134 (2000).
25. Montzka, S. A., Dutton, G. & Butler, J. H. The NOAA Ozone Depleting Gas Index: Guiding Recovery of the Ozone Layer, NOAA Earth System Research Laboratory. https://gml.noaa.gov/odgi/ (last accessed 21 Jan 2022).
26. Weatherhead, E. C. Detecting the recovery of total column ozone. *J. Geophys. Res.* **105**, 22201–22210 (2000).
27. Velders, G. J. M. & Daniel, J. S. Uncertainty analysis of projections of ozone-depleting substances: mixing ratios, EESC, ODPs, and GWPs. *Atmos. Chem. Phys.* **14**, 2757–2776 (2014).
28. Eyring, V. et al. Overview of the Coupled Model Intercomparison Project Phase 6 (CMIP6) experimental design and organization. *Geosci. Model Dev.* **9**, 1937–1958 (2016).
29. Jungclaus, J. H. et al. The PMIP4 contribution to CMIP6 – Part 3: The last millennium, scientific objective, and experimental design for the PMIP4 past1000 simulations. *Geosci. Model Dev.* **10**, 4005–4033 (2017).
30. Lean, J. L. Estimating solar irradiance since 850 CE. *Earth Space Sci.* **5**, 133–149 (2018).
31. Hersbach, H. et al. The ERA5 global reanalysis. *Q. J. R. Meteorol. Soc.* **146**, 1999–2049 (2020).
32. Brönnimann, S., Annis, J. L., Vogler, C. & Jones, P. D. Reconstructing the Quasi-Biennial Oscillation back to the early 1900s. *Geophys. Res. Lett.* **34**, L22805 (2007).
33. Laloyaux, P. et al. CERA-20C: a coupled reanalysis of the twentieth century. *J. Adv. Model. Earth Syst.* **10**, 1172–1195 (2018).
34. Weber, M. et al. The Brewer-Dobson circulation and total ozone from seasonal to decadal time scales. *Atmos. Chem. Phys.* **11**, 11221–11235 (2011).
35. Fioletov, V. E. & Shepherd, T. G. Seasonal persistence of midlatitude total ozone anomalies. *Geophys. Res. Lett.* **30**, 1417 (2003).
36. Brönnimann, S., Griesser, T. & Stickler, A. A gridded monthly upper-air data set from 1918 to 1957. *Clim. Dyn.* **38**, 475–493 (2012).
37. SPARC/IO3C/GAW, *Report on Long-term Ozone Trends and Uncertainties in the Stratosphere (LOTUS)* (Ed. Petropavlovskikh, I. et al, SPARC Report No. 9, GAW Report No. 241, WCRP-17/2018) (2019).
38. Rayner, N. A. et al. Global analyses of sea surface temperature, sea ice, and night marine air temperature since the late nineteenth century. *J. Geophys. Res.* **108**, 4407 (2003).
39. Steinbrecht, W., Claude, H., Köhler, U. & Hoinka, K. P. Correlations between tropopause height and total ozone: Implications for long-term changes. *J. Geophys. Res.* **103**, 19183–19192 (1998).
40. Keeble, J. et al. Evaluating stratospheric ozone and water vapour changes in CMIP6 models from 1850 to 2100. *Atmos. Chem. Phys.* **21**, 5015–5061 (2021).
41. Staehelin, J., Petropavlovskikh, I., De Mazière, M. & Godin-Beekmann, S. The role and performance of ground-based networks in tracking the evolution of the ozone layer. *Comptes Rendus Geoscience* **350**, 354–367 (2018).
42. Weber, M. et al. Total ozone trends from 1979 to 2016 derived from five merged observational datasets – the emergence into ozone recovery. *Atmos. Chem. Phys.* **18**, 2097–2117 (2018).
43. Weber, M. et al. Global total ozone recovery trends derived from five merged ozone datasets. *Atmos. Chem. Phys.* **22**, 6843–6859 (2022).
44. Coldewey-Egbers, M., Loyola, D. G., Lerot, C. & Van Roozendael, M. Global, regional and seasonal analysis of total ozone trends derived from the 1995–2020 GTO-ECV climate data record. *Atmos. Chem. Phys.* **22**, 6861–6878 (2022).

45. Dhomse, S. S. et al. Estimates of ozone return dates from Chemistry-Climate Model Initiative simulations. *Atmos. Chem. Phys.* **18**, 8409–8438 (2018).

46. Kuttippurath, J., Bodeker, G. E., Roscoe, H. K. & Nair, P. J. A cautionary note on the use of EESC-based regression analysis for ozone trend studies. *Geophys. Res. Lett.* **42**, 162–168 (2015).

47. Tarasick, D. et al. Tropospheric ozone assessment report: tropospheric ozone from 1877 to 2016, observed levels, trends and uncertainties. *Elem Sci Anth* **7**, 39 (2019).

48. Komhyr, W., Barrett, E., Slocum, G. & Weickmann, H. K. Physical sciences: atmospheric total ozone increase during the 1960s. *Nature* **232**, 390–391 (1971).

49. Ball, W. T., Chiodo, G., Abalos, M., Alsing, J. & Stenke, A. Inconsistencies between chemistry–climate models and observed lower stratospheric ozone trends since 1998. *Atmos. Chem. Phys.* **20**, 9737–9752 (2020).

50. Funk, J. F. & Gamham, G. L. Australian ozone observations and a suggested 24-month cycle. *Tellus* **14**, 378–382 (1962).

51. Hudson, R. D., Andrade, M. F., Follette, M. B. & Frolov, A. D. The total ozone field separated into meteorological regimes, part II: Northern Hemisphere mid-latitude total ozone trends. *Atmos. Chem. Phys.* **6**, 5183–5191 (2006).

52. Brönnimann, S. et al. Southward shift of the Northern tropical belt from 1945 to 1980. *Nat. Geosci.* **8**, 969–974 (2015).

53. Bojkov, R. D., Komhyr, W. D., Lapworth, A. & Vanicek, K. *Handbook for Dobson Ozone Data Re-evaluation*. WMO/GAW Global Ozone Research and Monitoring Project, Report No. 29, WMO/TD-no. 597 (1993).

54. Cornes, R., van der Schrier, G., van den Besselaar, E. J. M. & Jones, P. D. An ensemble version of the E-OBS temperature and precipitation datasets. *J. Geophys. Res. Atmos.* **123**, 9391–9409 (2018).

55. Vanicek, K., Dubrovsky, M. & Stanek, M. *Evaluation of Dobson and Brewer total ozone observtaions from Hradec Králové, Czech Republic, 1961–2002.* Publication of the Czech Hydrometeorological Institute, ISBN: 80-86690-10-5, Prague (2003).

56. Craddock, J. M. Methods of comparing annual rainfall records for climatic purposes. *Weather* **34**, 332–346 (1979).

57. Dobson, G. M. B. A photoelectric spectrophotometer for measuring the amount of atmospheric ozone. *Proc. Phys. Soc. London* **43**, 324–339 (1931).

58. Fabry, C. & Buisson, H. Etude de l'extremité ultra-violette du spectre solaire. *J. Phys. Rad., Série 6* **2**, 197–226 (1921).

59. Dobson, G. M. B. & Harrison, D. N. Measurements of the amount of ozone in the Earth's atmosphere and its relation to other geophysical conditions. *Proc. Roy. Soc. London* **A110**, 660–693 (1926).

60. Fabry, C. & Buisson, H. L'absorption de l'ultraviolet par l'ozone et la limite du spectre solaire. *J. Phys. Rad., Série 5* **3**, 196–206 (1913).

61. Dobson, G. M. B., Harrison, D. N. & Lawrence, J. Measurements of the amount of ozone in the Earth's atmosphere and its relation to other geophysical conditions, Part III. *Proc. Roy. Soc. London* **A122**, 456–486 (1929).

62. Dobson, G. M. B., Kimball, H. H. & Kidson, E. Observations of the amount of ozone in the Earth's atmosphere and its relation to other geophysical conditions, Part IV. *Proc. Roy. Soc. London* **A129**, 411–433 (1930).

63. Stickler, A. et al. The comprehensive historical upper-air network. *B. Amer. Meteorol. Soc.* **91**, 741–751 (2010).

64. Chapman, S. A theory of upper atmospheric ozone. *Mem. Roy. Meteor. Soc.* **3**, 103–125 (1930).

65. Dütsch, H.-U. *Photochemische Theorie des atmosphärischen Ozons unter Berücksichtigung von Nichtgleichge-wichtszustanden und Luftbewegungen.* Doctoral Dissertation, University of Zurich (1946).

66. Butchart, N. The Brewer-Dobson circulation. *Rev. Geophys.* **52**, https://doi.org/10.1002/2013RG000448 (2014).

67. Götz, F. W. P., Meetham, A. R. & Dobson, G. M. B. The vertical distribution of ozone in the atmosphere. *Proc. Roy. Soc.* **A145**, 416–446 (1934).

68. Vassy, A. & Vassy, E. Recherches sur l'absorption atmosphérique, I. *J. Phys. Radium* **10**, 75–81 (1939).

69. Farman, J. C., Gardiner, B. G. & Shanklin, J. D. Large losses of total ozone in Antarctica reveals seasonal ClOx/NOx interactions. *Nature* **315**, 207–210 (1985).

70. Stolarski, R. S. et al. Nimbus-7 satellite measurements of the springtime Antarctic ozone decrease. *Nature* **322**, 808–811 (1986).

71. Brewer, A. W. A replacement for the Dobson spectrophotometer? *PAGEOPH* **106–108**, 919–927 (1973).

72. Harris, N. R. P. et al. Trends in stratospheric and free tropospheric ozone. *J. Geophys. Res.* **102**, 1571–1590 (1997).

73. Ramaswamy, V., Schwarzkopf, M. D. & Shine, K. P. Radiative forcing of climate from halocarbon-induced global stratospheric ozone loss. *Nature* **355**, 810–812 (1992).

74. Lahoz, W. A., Errera, Q., Swinbank, R. & Fonteyn, D. Data assimilation of stratospheric constituents: a review. *Atmos. Chem. Phys.* **7**, 5745–5773 (2007).

Acknowledgements

Competing interests

The author declares no competing interests.

Additional information

Supplementary information The online version contains supplementary material available at https://doi.org/10.1038/s43247-022-00472-z.

Correspondence and requests for materials should be addressed to Stefan Brönnimann.

Peer review information *Communications Earth & Environment* thanks the anonymous reviewers for their contribution to the peer review of this work. Primary Handling Editor: Heike Langenberg. Peer reviewer reports are available.

Reprints and permission information is available at http://www.nature.com/reprints

Publisher's note Springer Nature remains neutral with regard to jurisdictional claims in published maps and institutional affiliations.